

# Att-Adapter: A Robust and Precise Domain-Specific Multi-Attributes T2I Diffusion Adapter via Conditional Variational Autoencoder

Wonwoong Cho<sup>1\*</sup> Yan-Ying Chen<sup>2</sup> Matthew Klenk<sup>2</sup> David I. Inouye<sup>1</sup> Yanxia Zhang<sup>2</sup>  
<sup>1</sup> Purdue University, West Lafayette, IN, 47906 <sup>2</sup> Toyota Research Institute, Los Altos, CA, 94022

## Abstract

*Text-to-Image (T2I) Diffusion Models have achieved remarkable performance in generating high quality images. However, enabling precise control of continuous attributes, especially multiple attributes simultaneously, in a new domain (e.g., numeric values like eye openness or car width) with text-only guidance remains a significant challenge. To address this, we introduce the **Attribute (Att) Adapter**, a novel plug-and-play module designed to enable fine-grained, multi-attributes control in pretrained diffusion models. Our approach learns a single control adapter from a set of sample images that can be unpaired and contain multiple visual attributes. The Att-Adapter leverages the decoupled cross attention module to naturally harmonize the multiple domain attributes with text conditioning. We further introduce Conditional Variational Autoencoder (CVAE) to the Att-Adapter to mitigate overfitting, matching the diverse nature of the visual world. Evaluations on two public datasets show that Att-Adapter outperforms all LoRA-based baselines in controlling continuous attributes. Additionally, our method enables a broader control range and also improves disentanglement across multiple attributes, surpassing StyleGAN-based techniques. Notably, Att-Adapter is flexible, requiring no paired synthetic data for training, and is easily scalable to multiple attributes within a single model.*

## 1. Introduction

Large pretrained T2I diffusion models [26, 29, 30, 33] have achieved remarkable success in generating high quality and realistic images based solely on text prompts. However, allowing users precise control over the generated content or tailoring it to a specific new domain remains challenging [8, 11, 31, 42]. For example, with the prompt “A photo of a woman smiling”, one might want to adjust specific facial attributes such as “width of nose” and “openness of eyes”

\*A significant portion of this work was performed during internship at Toyota Research Institute.

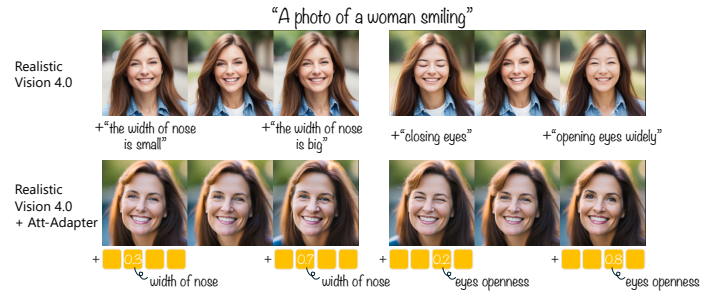


Figure 1. Att-Adapter enables continuous control (e.g., 0 to 1) over subtle visual details like nose width or eye openness, which are difficult to capture with discrete text-based conditioning.

by assigning specific numeric values to these attributes. As Fig. 1 demonstrates, current models like Stable Diffusion [30] (Realistic Vision 4.0<sup>1</sup>) fail to reliably control these fine-grained attributes, often misinterpreting or neglecting the specified modifications.

Early domain adaptation methods rely on text-based conditioning, either by optimizing text tokens [8, 31, 44] or fine-tuning T2I models using Low-Rank Adaptation (LoRA) [16]. However, text-only conditioning are inherently limited: texts often underspecifies visual details such as object type, perspective and style [17, 44], and existing methods typically handle only discrete attribute values.

Recent efforts attempt to address continuous attribute [3, 9, 22, 27]. AttributeControl [3] modifies CLIP embeddings but struggles with indescribable visual attributes (e.g., nose width) that rarely appear in text. Other methods, such as  $W_+$  Adapter[22] and PreciseControl [27], depend on pretrained StyleGAN latent spaces, making generation quality highly dependent on separately trained GANs. ConceptSlider [9] proposes a LoRA-based controller for indescribable visual attributes but requires paired data and trains separate models per attribute (Fig. 2). This limits its use to the case where only one attribute is paired while others remain unchanged, which makes it infeasible in unpaired multi-attribute data settings without generating synthetic pairs. However, generating synthetic paired data adds extra pre-

<sup>1</sup><https://huggingface.co/stablediffusionapi/realistic-vision-v40>

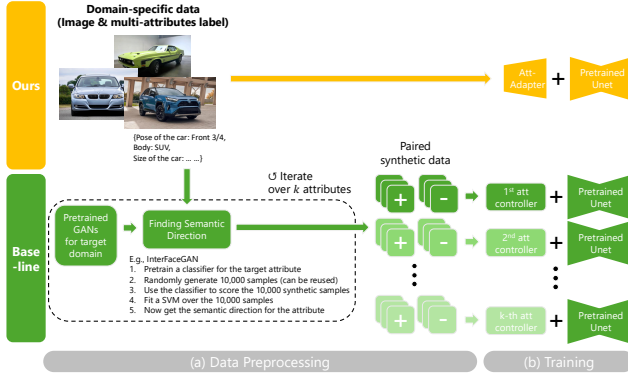


Figure 2. **Workflow comparison.** Unlike ConceptSlider [9], which demands paired data and separate models for each attribute, our approach supports unpaired multi-attribute control in a single framework. See Sec. 2 for details.

	Pretrained GANs	Continuous Attrs	Indescribable Visual Attrs	Multi-Attrs Training	Real Data Training
AttrCtrl [3]	✗	✗	✗	✗	✗
$W_+$ Adapter [22]	✓	✓	✓	✗	✗
ConceptSlider [9]	✓	✓	✓	✗	✗
ITI-GEN [44]	✗	✗	✓	✗	✓
LoRA [16]	✗	✗	✓	✓	✓
Ours	✗	✓	✓	✓	✓

Table 1. **Requirement and capability comparisons.** The left-most column shows a requirement while the others show benefits. Multi-Attrs indicate many attributes such as 20. Most baselines rely on a pretrained latent concept space where the synthetic attribute values are not directly from the real-world data.

processing steps and restricts performance to the quality of the data generator (e.g., StyleGAN). A detailed comparison with existing methods is listed in Table 1.

In this paper, we propose **Att-Adapter**, a novel plug-and-play adapter that enables precise control over multiple attributes in pretrained diffusion models. As illustrated in the top row of Fig. 2, Att-Adapter learns multi-attribute control from unpaired real data by leveraging a decoupled cross-attention module [43] to effectively fuse conditions from different modalities (e.g., view angle, size, style). We found that directly mapping multiple attributes with a naive MLP leads to overfitting (Fig. 8 and Table 5); To this end, we incorporate a Conditional Variational Autoencoder (CVAE) [37, 46] to improve robustness against overfitting. By performing an approximate Bayesian inference [20], the CVAE can naturally regularize Att-Adapter via its KL divergence term. This not only mitigates overfitting but also smooths the conditional representation, modeling the natural randomness for given attribute condition.

Extensive experiments on face and car datasets demonstrate that Att-Adapter outperforms state-of-the-art methods in both continuous and discrete attribute control. Our contributions are as follows:

- **Unpaired Multi-Attribute Control:** Att-Adapter simultaneously controls multiple attributes from unpaired data,

eliminating the need for costly paired samples.

- **Continuous and Indescribable Attribute Manipulation:** Our approach precisely controls subtle visual details that are difficult to describe textually.
- **Robust Control:** The integration of a CVAE mitigates overfitting, ensuring stable and accurate attribute control.

## 2. Related Works

**Single Attribute Control for T2I Generation.** Diffusion models (DMs) [6, 15, 36] are one of the widely-used text-to-image generative models due to its impressive performance. To customize DMs for a particular domain or new concept, fine-tuning the U-Net is a common approach [21, 31], although it can lead to catastrophic forgetting [24, 25]. Instead of retraining all model parameters, Low-Rank Adaptations (LoRA) [16], adds trainable low rank decomposition matrices to each layer of a frozen model, significantly reducing trainable parameters while maintaining performance. Other methods, such as DreamBooth [31] and Textual Inversion [8], modify text embeddings of pretrained T2I models [8, 31, 44]. Both LoRA and text embedding approaches require training a new LoRA network or token for each attribute. Additionally, they struggle to represent continuous attribute values without discretization.

**Multi-Attribute Control for T2I Generation.** Existing methods often combine individually trained LoRAs through weighted averaging, which can lead to concept vanish or distortion [11, 21, 24, 42]. Approaches like Mix-of-Show [11] and Lora-composer [42] attempt to address this but still require separate LoRAs, limiting scalability and forcing discretization of continuous attributes.

Text embedding modification methods face similar challenges. Custom Diffusion [21] uses unique tokens for each concept, optimizing multiple embeddings but lacking continuous control and extrapolation. DreamDistribution [45] learns prompts from reference images, creating diverse outputs but without fine control over continuous attributes. ITI-GEN [44] addresses catastrophic forgetting with prompt engineering, using pretrained parameters for consistency and balance sampling. These methods struggle in representing continuous attribute and require discretization. Furthermore, the token embeddings need to be trained with all the attribute combinations, significantly limiting its scalability.

**Continuous Attribute Control.** Several methods aim to enable attribute control on a continuous scale [3, 9, 22, 27]. Pretrained Generative Adversarial Networks (GANs) [10] such as StyleGAN [18] have been extensively explored for continuous attribute control. For example, InterFaceGAN [35], GANSpace [13], and StyleSpace [40] can be used to enable the attribute controls over the pretrained GAN’s space.  $W_+$  Adapter [22] and PreciseControl [27]

link pretrained diffusion models with the pretrained GANs’  $W_+$  space [13, 35, 40]. However, their performance is constrained by the quality of the  $W_+$  space. Furthermore, if there is no public pretrained GANs for specific domains, they require training new GANs from scratch.

ConceptSlider [9] trains LoRA adapters for fine-grained control of indescribable visual concepts. Unlike ConceptSlider, our method supports multi-attribute control in both training and sampling without requiring separate models for each attribute. Moreover, ConceptSlider relies on paired data, which is often synthesized and can degrade performance when used in unpaired settings. In contrast, our approach remains effective with real data, making it more flexible and practical. AttributeControl [3] proposes learning a certain attribute (e.g., old) in the CLIP text embedding space by contrasting the attribute-related words (e.g., old and young). However, their method is inherently not suitable for attributes that are difficult to describe in text. In contrast to existing works, our method does not rely on paired data and a pretrained latent embedding space.

### 3. Method

In this section, we first describe the naive version of Att-Adapter with a simple MLP network, where personal identity overfitting is observed. We then describe Att-Adapter with conditional variational autoencoder (CVAE) to mitigate the undesirable overfitting issue.

#### 3.1. Problem Formulation

Att-Adapter takes a set of domain-specific attributes  $C$  as input with the text prompt  $Y$ , modeling  $p(X|Y, C)$ . Our method is designed to support multiple attributes. Hence, we can scale to an unlimited number of conditions with negligible increase in memory usage. For example,  $C_1, C_2, C_3$  and  $C_4$  could be ‘height of eyes’, ‘width of nose’, ‘age’, and ‘probability of Asian’, and all of the attributes can be trained altogether, which can be represented as  $p(X|Y, C_1, C_2, C_3, C_4)$ .

Formally, similar to previous works [14, 38], we can approximate  $p(X|Y, C)$  with the reverse diffusion process with timestep  $t$  by:

$$\begin{aligned} \nabla_X \log p(X(t)|Y, C) \approx \\ \epsilon_\theta(X(t)) + w(\epsilon_\theta(X(t), Y, C) - \epsilon_\theta(X(t))) \end{aligned} \quad (1)$$

where  $\epsilon_\theta(X(t))$  and  $\epsilon_\theta(X(t), Y, C)$  are unconditional and conditional diffusion models, respectively. Now, the question boils down to how to implement  $\epsilon_\theta(X(t), Y, C)$ .

#### 3.2. Att-Adapter

To model the conditional with diffusion models, i.e.,  $\epsilon_\theta(X(t), Y, C)$ , we adopt the decoupled cross-attention

module [43] as it is highly effective in combining two different conditions with different modalities. Specifically, the decoupled cross-attention modules for attribute feature injection are formulated as:

$$\text{Attention}(Q, K_{\text{text}}, V_{\text{text}}) + \lambda \text{Attention}(Q, K_{\text{attr}}, V_{\text{attr}}), \quad (2)$$

where  $\lambda$  controls the strength of the attribute, and the key and value for attributes come from the multi-attributes condition through Att-Adapter, i.e.,  $K_{\text{attr}} = W_k \text{AttAdapter}(c)$  and  $V_{\text{attr}} = W_v \text{AttAdapter}(c)$ .

In the following sections, we first describe our Att-Adapter using a naive MLP-based mapping network and summarize our key observations. We then introduce our enhanced Att-Adapter with a CVAE module to overcome overfitting in multi-attribute control generation.

##### 3.2.1. Naive Att-Adapter with a MLP Mapping

A naive version of Att-Adapter for multi-attributes control is to have a simple linear function  $g$  that maps the multiple attributes  $C$  into the input space of the pretrained decoupled cross-attention modules. More precisely,  $g$  outputs the input of the layer norm [2], and the output of the norm layer is fed into the decoupled cross-attention module. The linear function  $g$  and the decoupled cross-attention modules are optimized with the denoising objective function, i.e.,

$$\mathcal{L}_{\text{denoising}}(x_t, t, y, c; g) = \mathbb{E} [\|\epsilon - \epsilon_\theta(x_t, t, y, g(c))\|^2], \quad (3)$$

where  $\epsilon_\theta$  is pretrained diffusion models [30].

We find that the naive Att-Adapter can control multiple attributes and can be integrated well with text conditioning, benefiting from the decoupled cross-attention module to merge multimodal conditions. However, we observed overfitting when fixing attribute values  $C = c$  while varying the random Gaussian sample at the timestep  $T$ . In this case, diffusion models tend to generate visually similar images (see w.o. CVAE in Fig. 8 and Table 5). This is problematic since a single set of  $c$  does not correspond to a unique human subject. Many individuals may share similar attributes such as nose width. To address this, we propose an enhanced Att-Adapter that overcomes overfitting while maintaining precise attribute control.

##### 3.2.2. Att-Adapter with CVAE

To mitigate the undesirable overfitting, we design Att-Adapter as a one-to-many mapping function from  $C$ . To this end, we introduce Conditional Variational Autoencoder [37, 46] (CVAE) that can naturally regularize the model parameters from overfitting and can learn the latent space  $Z$ . To be specific, the KL-divergence term with the prior distribution can make the conditional latent

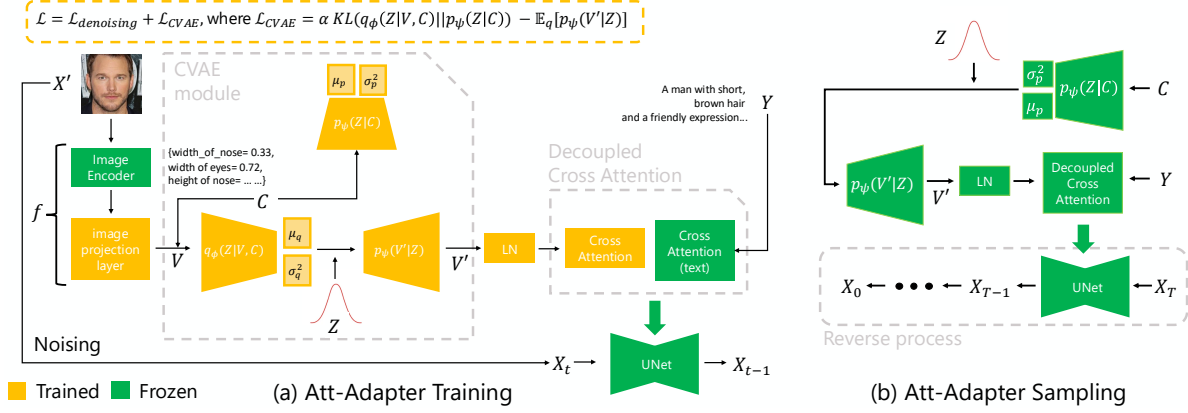


Figure 3. An illustration of the training process of Att-Adapter. (a) shows the training process for the Att-Adapter with CVAE. Our model learns a single multi-attribute control model given a set of sample images with different values for attribute  $C$  (i.e., width of nose/eyes). (b) shows the sampling process of Att-Adapter. Our CVAE decoder  $p_\psi(V'|Z)$  takes a random sample by conducting reparameterization trick from the conditional prior  $p_\psi(Z|C)$  taking  $C$  as input and having been learned to output the mean and the variance of the isotropic Gaussian. We empirically show that our CVAE modeling is effective in preventing overfitting as we intended.

space smoother, preventing the over-simplified representation for  $C$ . This is because VAEs [20] perform approximate Bayesian inference, promoting generalization rather than memorizing or simplifying the data distribution.

The overview of Att-Adapter is provided in Fig. 3 (a). We use the pretrained image encoder, such as CLIP [28] or a face recognition model [4, 5, 12]. Inspired by [37], our CVAE module includes a variational encoder  $q_\phi(Z|V, C)$ , a conditional prior network  $p_\psi(Z|C)$ , and a decoder  $p_\psi(V'|Z)$ . We empirically remove the condition  $C$  from the decoder, since the conditional prior  $Z$  already contains the information of  $C$ . Complete derivations for the CVAE ELBO can be found in [37].

Let  $V$  and  $V'$  be input and output of the CVAE module, where  $V$  can be obtained from the image encoding branch  $f$ . The output  $V'$  is fed into the denoising UNet through the decoupled cross attention module, similar to the simple version of Att-Adapter.

In accordance with the general CVAE setup, we assume that the prior and the posterior networks follow a Multivariate Gaussian which means both the prior and posterior networks estimate the Gaussian parameters  $\mu$  and  $\sigma$ . As opposed to [46], we assume an isotropic Gaussian only for the prior but not for the posterior as it is unusual in the image domain in practice, i.e.,  $q_\phi(Z|V, C) \sim \mathcal{N}(\mu, \Sigma)$ , where  $\Sigma = \text{diag}(\sigma_1^2, \sigma_2^2, \dots)$  and  $p_\psi(Z|C) \sim \mathcal{N}(\mu, \sigma^2 \mathbf{I})$ .

During the training, our variational encoder  $q_\phi(Z|V, C)$  takes the multi-attributes condition with the image feature and approximate the gaussian parameters  $\mu_q$  and  $\sigma_q$  for the given condition. Our decoder  $p_\psi(V'|Z)$  then takes the reparameterized sample and outputs  $V'$ . The conditional prior network  $p_\psi(Z|C)$  is trained together and learns to produce conditional prior distributions  $\mu_p$  and  $\sigma_p$ . The evidence

lower bound (ELBO) of the CVAE is defined as:

$$\begin{aligned}
 \text{ELBO} &\triangleq \\
 & - \text{KL}(q_\phi(z|v, c) || p_\psi(z|c)) + \mathbb{E}_{q_\phi(z|v, c)} [\log p_\psi(v'|z, c)] \\
 & \leq \log p(V = v | C = c).
 \end{aligned} \tag{4}$$

**Training Objectives.** In conjunction with the CVAE objective, the standard denoising objective is applied, i.e.,  $\mathcal{L}_{\text{denoising}}(x_t, t, y, c, x') = \mathbb{E} [\|\epsilon - \epsilon_\theta(x_t, t, y, c, x')\|^2]$ . The final objective for optimizing our proposed Att-Adapter is defined as:

$$\begin{aligned}
 \mathcal{L}(x_t, t, c, y, x') = \\
 \mathcal{L}_{\text{CVAE}}(f(x'), c; \alpha) + \mathcal{L}_{\text{denoising}}(x_t, t, y, c, x'), \tag{5}
 \end{aligned}$$

where  $\mathcal{L}_{\text{CVAE}}(f(x'), c; \alpha)$  is negative ELBO in Eq. 4, where  $\alpha$  is a coefficient for the KL term, and  $f$  is a chain of functions to extract the image feature  $v$  as shown in Fig. 3 (b). The full set of parameters to be updated is colored yellow in the figure while the green parts are frozen. We empirically use  $\alpha = 0.0001$ .

Unlike the simple version of Att-Adapter that is trained only with the denoising objective, Att-Adapter with CVAE is designed to be robust against overfitting by minimizing  $\mathcal{L}_{\text{CVAE}}$  together with the denoising loss.

**Reparameterization and Sampling.** Following the CVAE literature [20], we use the reparameterization trick for both training and sampling process. During training, reparameterization is applied for the posterior  $q_\phi$  to make the sampling process differentiable. During sampling, reparameterization is used to sample from the conditional prior distribution  $p_\psi(Z|C)$  as shown in Fig. 3 (b).

## 4. Experiments

More details on the data are in the appendix (Sec. A).

### 4.1. Dataset and Preprocessing

**FFHQ:** FFHQ [18] is a high-quality public face dataset. To use the data for finetuning Text-to-image diffusion models, we get a caption per image by using ChatGPT [1]. We pre-processed 20 facial attributes: 13 attributes for facial compositions, one attribute for age, and 6 attributes for race. Specifically, we first obtain head pose information (pitch, roll, and yaw)<sup>2</sup> and use them to get frontal view face images; We extract 16,336 images out of 70,000 images, which are used as our fine-tuning data. Next, we use 68 landmarks per image from dlib [19] to obtain the information about facial composition. For example, ‘the gap between eyes’ and ‘width of mouth’. For age and race extraction, we use deepface [34] with a detector RetinaFace [5].

**EVOX:** We used a commercial grade vehicle image dataset from EVOX<sup>3</sup>. The dataset includes high-resolution images across multiple car models collected from 2018 to 2023, totally 2030 images.

### 4.2. Evaluation Setup

This section defines our baselines and the metrics used for comparison. As shown in Table 1, existing methods use two different settings for attribute control: *absolute* and *latent*. In the absolute setting, attribute values are explicitly provided using real-world data (e.g., absolute distances measured from images). In contrast, the latent setting assigns attribute values within a predefined concept space, such as those in GANs and CLIP, where values can only be manipulated within the given space.

#### 4.2.1. Baselines

**Baselines (Latent Control).** Baseline methods for precise continuous attribute control require positive and negative paired data for training and often need a pretrained concept space [3, 9, 22] as discussed in Sec. 2.

**S-I-GANs.** This baseline is implemented by combining StyleGAN 2 [18] and InterFaceGAN [35]. We start from the 16,336 images from Sec. 4.1 and their attribute labels. We first use the e4e [39] encoder to project the real images onto the  $W_+$  space. We then fit a SVM to get the semantic control direction per attribute by using the projected data and the corresponding labels.

**$W_+$  Adapter [22].** The retrieved semantic directions from InterFaceGAN are used to get the negative and positive samples to evaluate.

**ConceptSlider [9].** The LoRA-based controllers from ConceptSlider require paired data for training. Since we do not usually have paired data for domain-specific attributes, e.g.,

face, we use the generated synthetic paired data from S-I-GANs to train ConceptSlider. We also train ConceptSlider (unpair) without paired data. Briefly, 1000 positive and another 1000 negative unpaired images are used.

**AttrCtrl. [3]** They do not use any image data to train their controller, so we make a text pair following the instructions. For example, the prompt target is set as ‘man’ and the positive and the negative prompts are ‘man with big gap between eyes’ and ‘man with small gap between eyes’.

**Baselines (Absolute Control).** Next, we compare our performance with baseline methods that share the same data setting as ours; unpaired multi-attribute data.

**LoRA [16].** Since ConceptSliders, which are based on LoRA, are not designed for training with unpaired data, we introduce another baseline that natively supports unpaired multi-attributes training. This approach first discretize continuous values and finetune using special tokens. For example, if two attributes have values of 0.2 and 0.4, the LoRA’s condition is represented as ‘Z2 Y4’. Fig. 14 in the appendix provides a detailed example. To achieve optimal results, we apply LoRAs to both UNet and text encoder.

**ITI-GEN [44].** ITI-GEN is not scalable for handling multiple conditions with numerous categories. Our goal is to model a conditional distribution that takes 20 attributes along with a text prompt, denoted as  $p(x|y, c_1, c_2, \dots, c_{20})$ . To achieve this within the ITI-GEN framework, we first generate inclusive prompts separately for every pair of attributes and model distributions such as  $p(x|y)$ ,  $p(x|c_1, c_2)$ , ..., and  $p(x|c_{19}, c_{20})$ . We then approximate the full conditional by merging the prompt information by averaging in the prompt embedding space (naive) or by leveraging Composable Diffusion Models (CDM) [23] in the score space.

#### 4.2.2. Measures

**Baselines (Latent Control).** In this setting, attribute values come from the pretrained GANs’ latent space rather than the actual facial attributes, making direct comparisons between input  $c$  and predicted  $\hat{c}$  (from the generated image) infeasible. Instead, we generate 200 paired images per attribute (e.g., closed vs. open eyes) and compare estimated attributes  $\hat{c}_{neg}$  and  $\hat{c}_{pos}$  using dlib [19]. A higher score indicates a broader control range. We evaluate 13 individual attributes (2,600 images) and 10 multi-attribute combinations (2,000 images), applying a recommended or broader conditioning range than the original implementation (Sec. A in the appendix).

We measure the Control Range (CR) as the L1 distance between the target attributes of  $\hat{c}_{neg}$  and  $\hat{c}_{pos}$ , where a higher value indicates better expressivity of the model with respect to the target attribute. Disentanglement Performance (DIS) is evaluated as the proportion of changes in the target attribute relative to total changes, with higher values indicating better disentanglement.

<sup>2</sup><https://github.com/DCGM/ffhq-features-dataset>

<sup>3</sup>For more information, see <https://www.evostock.com/>.

**Baselines (Absolute Control).** Baselines in this setting take a real unpaired condition  $c$ , allowing direct performance evaluation by comparing input  $c$  with estimated  $\hat{c}$  from the generated image using dlib [19]. The lower error indicates better alignment between the generated images and the control attribute values.

We also measure the accuracy of race and age using deepface [34] and Retinaface [5]. The estimated age is compared with the input age via L1 distance, while race is evaluated using cross-entropy (lower is better).

Next, we measure the CLIP score [28] to see if the generated images keep the pretrained knowledge. Lower scores suggest knowledge loss. We also use ChatGPT to verify alignment with the query “Does the prompt ‘[PROMPT]’ correctly describe the image? Shortly answer yes or no.”

For evaluation, we predefine 30 text prompts representing pretrained knowledge (which rarely/never exist in the finetuning data), e.g., ‘A marble sculpture of a man/woman’. For each prompt, we randomly sample 50 combinations of 20 attributes, totaling 1,500 test samples. Details can be found in Sec. A in the appendix.

For EVOX data, ChatGPT assesses whether the model correctly applies pose and body attributes to generated car. we use SegFormer [41] to measure the size accuracy. Briefly, we generate a pair of cars by giving the same random noise but different size conditions. Segmentation mask are then compared to quantify size differences.

### 4.3. Evaluations

#### 4.3.1. Baselines (Latent Control)

We measure how well the target attribute is applied to the generated images in both single and multiple attributes. As shown in Table 2, our results outperform the baselines in both CR and DIS in the single and multiple attribute settings. The better disentanglement (DIS) scores of ours can be seen as a benefit of multi-attributes training. That is, all attributes are trained together learning the correlation between the attributes. This indicates that Att-Adapter can learn each attribute more precisely, which is also verified as the better CR score of ours. This is not surprising because the bigger the facial expressions are, the correlation between the attributes get bigger which is harder to learn without considering other attributes together.

The better CR score is also attributed to the fact that Att-Adapter can be trained with the real image and the real attributes as opposed to the baselines. Recall that the baselines require the pretrained GANs’ space which essentially constraints their performance, i.e., both  $W_+$ Adapter and ConceptSliders are worse than S-I-GANs. This makes sense as the training dataset of  $W_+$ Adapter and ConceptSliders are the synthetic paired images generated by S-I-GANs.

Note that AttrCtrl performs not well in our evaluation protocols, as the method is not well-suited for visual at-

tributes that cannot be easily described in text.

Fig. 4 shows the qualitative results align with Table 2. Both  $W_+$ Adapter and ConceptSliders show that the person identity across column is affected (low DIS) while the target attribute effects are weaker than ours (low CR). S-I-GANs shows relatively good attribute control performance as shown in the stronger target attribute effects than other baselines. For example, the rightmost three columns show bigger mouth openness than  $W_+$ Adapter and ConceptSliders. This also reveals the inherent limitation of the them; the pretrained GANs’ performance cascades/upperbounds. Ours, on the other hand, shows the best performance in applying the target attribute better while having minimal change for the remaining attributes.

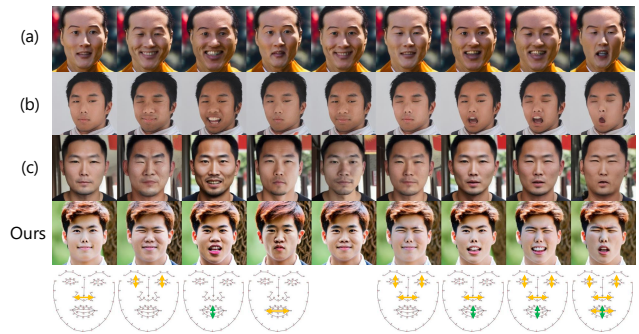


Figure 4. Best performing Latent Control Baselines; (a)  $W_+$ Adapter (b) S-I-GANs (c) ConceptSlider. Ours shows better performance in applying the target attribute with minimal change for the rest. The green and yellow arrows respectively indicate positive and negative direction controls.

		Ours	ConceptSliders		AttrCtrl	$W_+$ Adapter	S-I-GANs
			Pair	Unpair			
CR (↑)	Single	<b>67.87</b>	26.73	8.64	9	26.59	49.45
	Multi	<b>90.39</b>	31.35	10.5	20.78	40.76	68.4
DIS (↑)	Single	<b>29.8%</b>	17.5%	10.4%	7.6%	15.8%	21.8%
	Multi	<b>32.3%</b>	19.8%	12.2%	11.4%	18.5%	20.1%

Table 2. Latent Control Baselines. CR indicates the control range of the attribute that each model is capable of, and DIS denotes disentangling performance. Our results outperform the baselines in both measures.

#### 4.3.2. Baselines (Absolute Control)

Fig. 5 shows the performance of ours and the baselines. Compared to the baseline column in the yellow box in the center, only one attribute is changed for each column. The changed target attribute is presented in the bottommost row.

Fig. 5 (a) ITI-GEN does not show meaningful semantic changes for both facial compositing attributes and age. This is because ITI-GEN is limited in combining multiple conditions post hoc, as described in details in sec. 4.2. It is also shown in Table 3 (B) and (C). Both naive and cdm methods

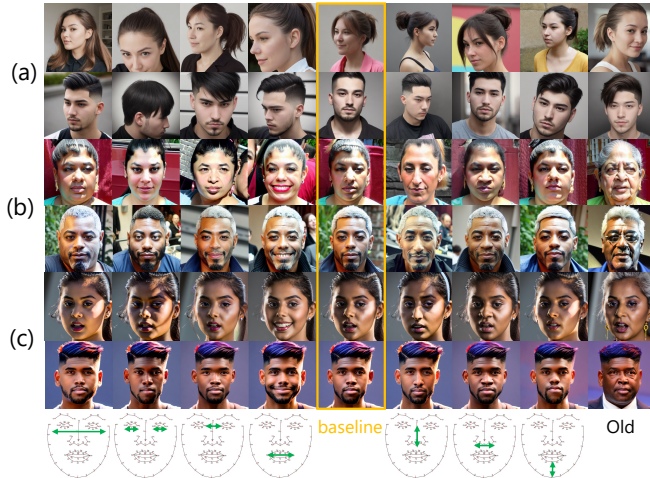


Figure 5. Qualitative results using Absolute Control baselines. From the top, (a) ITI-GEN, (b) LoRA, and (c) Att-Adapter.

	Finetuned knowledge (L1↓)			Pretrained knowledge (↑)	
	Facial comp.	Age	Race	CLIP	ChatGPT
(A)	17.48	10.0	0.48	0.270	72%
(B)	52.16	8.8	1.77	<b>0.288</b>	79%
(C)	70.09	9.3	2.06	0.286	<b>84%</b>
Ours	<b>15.57</b>	<b>8.0</b>	<b>0.36</b>	0.283	78%

Table 3. Quantitative results using Absolute Control baselines. (A) LoRA, (B) ITI-GEN [44] (naive), (C) ITI-GEN (CDM [23]).

are not correctly applying the finetuned knowledge to the generation process, even though it maintains the pretrained knowledge well. This is because ITI-GEN is not scalable to many attributes by design (e.g., 20 in our experiments)

**LoRA v.s. Ours in FFHQ.** Fig. 5 (b) and (c) show the results of LoRA and ours. The results from both methods show decent performance in applying the target attribute while maintaining the original knowledge. However, Att-Adapter outperforms LoRA in many aspects.

First of all, their visual fidelity is not as good as ours in (c). This is because Att-Adapter can naturally combine two different conditions (i.e., text and the attributes) by leveraging the decoupling cross-attention layer and the strong embedding power of the pretrained image encoder. Secondly, the performance for applying the facial attributes is worse than ours. For example, in the row (b) in the sixth column from the left, the height of nose changes a lot of other visual features together such as face length and mouth shape, while ours does less. Similarly, in Table 3, ours shows better performance in correctly applying the given facial component attributes. Third, our Att-Adapter shows better performance in correctly applying the given race attribute as shown in Table 3 by the lower cross entropy. The better performance of Att-Adapter over the baseline in the

race attribute can be found in Fig. 6. This can be observed by comparing the fourth and sixth columns of (a), which shows that LoRA is confused with the generation of white and Hispanic.

We believe this is caused by the fundamental limitation of discretization. It shrinks the amount of the original information which can cause distortions of the correlation between the facial features. Furthermore, discretizing the value is inherently limited in extrapolating the attributes. Please see Fig. 13 in the appendix, which shows the advantage of our method over the LoRA baseline.

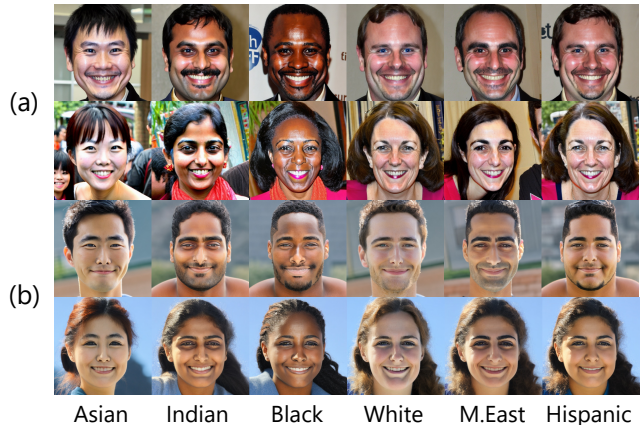


Figure 6. Qualitative Baseline comparisons on race. From the top, (a) LoRA, and (b) Att-Adapter. The prompts of “A photo of a woman smiling” and “A photo of a man with shadow fade hair style” are used for the woman images and the man images.

**LoRA v.s. Ours in EVOX.** To demonstrate the generalizability of Att-Adapter beyond human face dataset, we conducted an experiment on EVOX dataset. Fig. 7, shows the results. First, both Att-Adapter and LoRA generate well the discrete attributes such as pose, e.g., front view, and body of the car, e.g., SUV. For example, on the first macro row, both models consistently generate SUVs. However, we can see that ours show better performance in controlling the continuous attribute like size of the car, compared to LoRA. Moreover, we can see that Att-Adapter shows better performance in maintaining the pretrained knowledge. For example, given the prompt of “A photo of a rainbow car”, the results from ours show stronger prompt effects.

These observations can be verified by Table 4 quantitatively. While the performance of LoRA and Att-Adapter is comparable in Pose and Body, Att-Adapter outperforms the baseline in continuous attributes and maintaining the original knowledge, which is consistent with FFHQ results.

	Pose (↑)	Body (↑)	Size (↑)	CLIP (↑)
LoRA	<b>99%</b>	75%	67%	0.22
ours	98%	<b>76%</b>	<b>95%</b>	<b>0.24</b>

Table 4. Absolute control baseline comparisons in EVOX dataset.

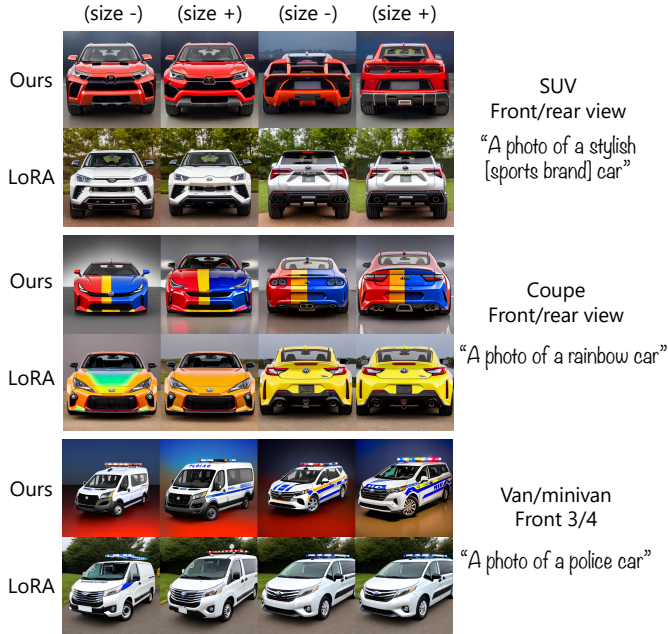


Figure 7. Absolute control baseline comparisons in EVOX dataset. [sports brand] refers to a well-known luxury sports car manufacturer.

(Iter)	w.o. CVAE			with CVAE (200k)
	(20k)	(50k)	(200k)	
CR ( $\uparrow$ )	47.04	62.06	78.27	78.59
ID Sim ( $\downarrow$ )	6.0%	27.1%	28.5%	6.2%

Table 5. ID Sim stands for the average face verification scores by DeepFace (Facenet512) between all the pairs of 100 randomly generated images while feeding a fixed attribute conditions  $c$ . The results show that CVAE regularizes Att-Adapter from overfitting.

$(\lambda.)$	Finetuned knowledge ( $\downarrow$ )			Pretrained knowledge ( $\uparrow$ )	
	Facial comp.	Age	Race	CLIP	ChatGPT
0.0	69.43	8.8	1.3	<b>0.298</b>	<b>97%</b>
0.5	28.96	8.5	0.50	0.293	94%
0.7	17.96	<b>8.0</b>	0.38	0.288	89%
0.9	<b>15.57</b>	<b>8.0</b>	<b>0.36</b>	0.283	78%

Table 6. Performance reports with different  $\lambda$ s. The lower the  $\lambda$  is, the stronger the pretrained knowledge affects the generation process while relatively weakening the influence of Att-Adapter.

#### 4.4. Analysis and Application

**Att-Adapter with and without CVAE.** We conducted additional ablation studies that compare the CVAE with an alternative MLP. Fig. 8 shows that using CVAE naturally regularizes the Adapter from overfitting. The results without CVAE shows low image diversity and convergence to similar facial appearances. Consistent patterns are observed in Table 5. Although more training iterations improve attribute control, the person ID diversity significantly decreases.

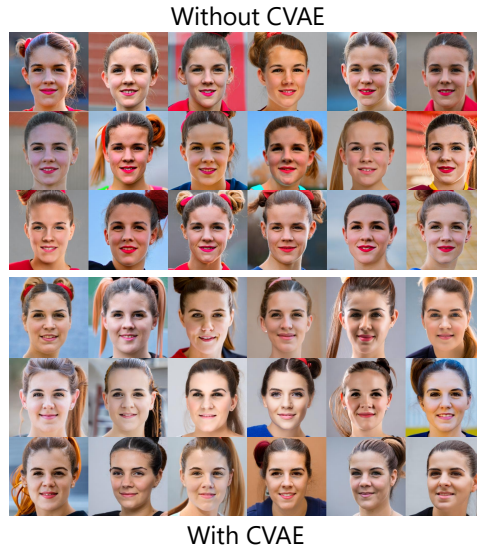


Figure 8. Overfitting phenomenon. All of the conditions such as the attributes and the text prompt are fixed while the random sample such as  $x_T$  and  $\epsilon \sim N(0, I)$  for reparameterization are changed. It is not surprising that the generated images look similar as the given  $c$  is fixed. However, the fixed  $c$  does not necessarily mean the fixed person ID. The output person’s identity is saturated without CVAE setting, which is not ideal as shown in Table 5.

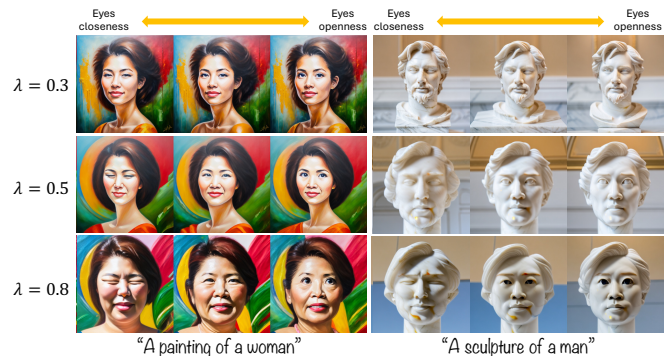


Figure 9. Qualitative explorations on the effects of  $\lambda$ .

$\lambda$  **during the sampling.** As shown in Eq. 2 in the main paper,  $\lambda$  controls the strength of Att-Adapter when merging the information from different input conditions. Intuitively, by reducing  $\lambda$ , we can expect that Att-Adapter will affect the generation process less. This can be verified by looking at Fig. 9. When  $\lambda = 0.3$ , we can see that the effect of text prompt is strong while the attribute effect is weak. For example, the sculptures does not look like the given attribute, ‘Asian’. When  $\lambda = 0.8$ , the effect of Att-Adapter (where the finetuning knowledge passes through) gets stronger as we can see that the results in the third row have more human-like texture and face-cropped view. The quantitative results can be found in Table 6. We can first see that pretrained knowledge, measured by CLIP and Chat-

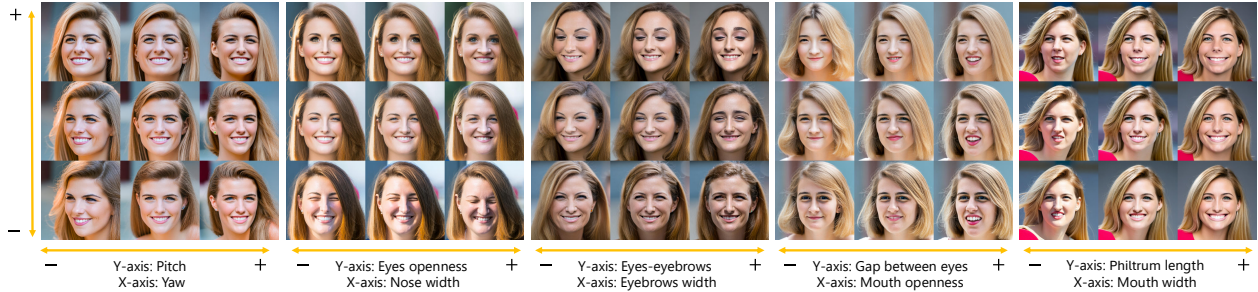


Figure 10. Additional multi-attributes control examples. A prompt of “A woman smiling” is used to generate. Only a single Att-Adapter is used for all of the controlling examples.

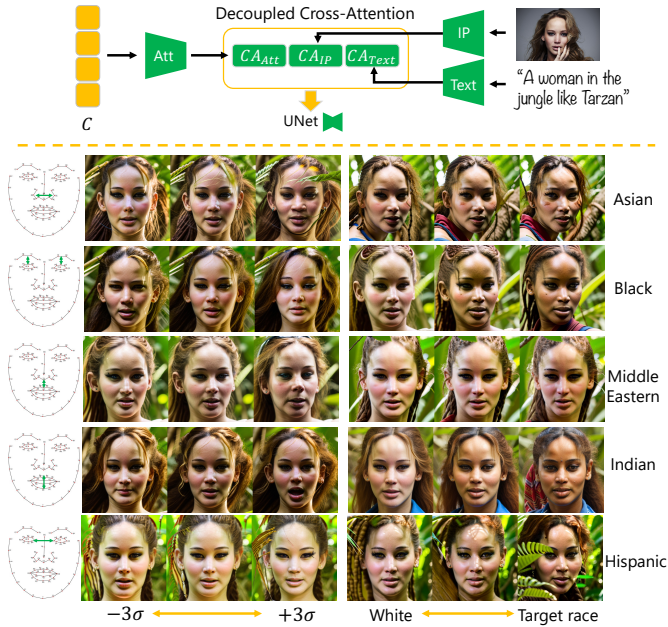


Figure 11. Examples on adapting both IP- and Att-Adapter to pre-trained diffusion models to take an image as input.  $\sigma$  is pre-computed standard deviation per attribute from the finetuning data.

GPT is maintained better with lower  $\lambda$ . The higher the  $\lambda$  is, on the other hand, we can expect the stronger effects of the fine-tuned knowledge, in exchange for losing the pretrained knowledge.

**Exploring training settings.** We explore several different settings of our method. The details are in Sec. C in the appendix. Some of the takeaways from the experiments are as follows. 1) Model performance is converged around 200k iterations with batch size of 4. 2) Embedding dimension  $d$  (i.e.,  $Z \in \mathbb{R}^d$ ) needs to be bigger than 128 such as 512 or 2048. 3) The performance difference between isotropic and non-isotropic gaussian prior is marginal.

**Controlling multiple attributes.** Fig. 4 and Fig. 10 shows the superior performance of Att-Adapter in controlling

multi-attributes. More examples and a detailed explanation about the additional attributes yaw and pitch are provided in the appendix (Sec. E.1).

**Application: Augmenting Other Adapters.** To show more potential applications of Att-Adapter, we connect IP-Adapter[43] with Att-Adapter to take an image input while controlling the attributes of the input image by Att-Adapter. Details are shown in the top of Fig. 11. During the inference, we attach IP-Adapter and Att-Adapter together to pretrained Diffusion Models. The Decoupled Cross-Attention layer is extended to  $CA(Q, K_{text}, V_{text}) + \lambda_1 CA(Q, K_{attr}, V_{attr}) + \lambda_2 CA(Q, K_{ip}, V_{ip})$ , where  $\lambda_1$  and  $\lambda_2$  determine the strength of Att-Adapter and IP-Adapter, respectively. We use 0.35 and 1.0 in practice. Interestingly, as shown in Fig. 11, the attribute information from Att-Adapter can be harmonized well with IP-Adapter, even though not trained together.

We also show the results of combining LoRA finetuned for a person ID with Att-Adapter in the appendix (Sec. B).

## 5. Conclusion and Discussion

We present Att-Adapter for T2I diffusion models to enable fine-grained attribute control by adjusting continuous numeric values. Att-Adapter leverages decoupled cross-attention module to merge the conditions under different modalities. CVAE is further introduced to mitigate the overfitting issue. Different from the baselines, Att-Adapter can be trained without any paired data while can learn multi-attributes at once. The learned adapter allows meaningful and precise manipulation of attributes in the targeted domain. The experiment results demonstrate that Att-Adapter can more accurately control continuous attribute variables across multiple datasets compared to the baselines.

**Potential Societal Impacts.** This study uses face dataset in the experiments for fair comparisons with the prior works. However, the approach is generic for other objects such as cars as demonstrated in the paper. We encourage a shift towards use cases in object manipulation and product design to reduce ethical concerns about privacy and discrimination.

## References

- [1] Josh Achiam, Steven Adler, Sandhini Agarwal, Lama Ahmad, Ilge Akkaya, Florencia Leoni Aleman, Diogo Almeida, Janko Altenschmidt, Sam Altman, Shyamal Anadkat, et al. Gpt-4 technical report. *arXiv preprint arXiv:2303.08774*, 2023. 5, 12
- [2] Jimmy Lei Ba, Jamie Ryan Kiros, and Geoffrey E Hinton. Layer normalization. *arXiv preprint arXiv:1607.06450*, 2016. 3
- [3] Stefan Andreas Baumann, Felix Krause, Michael Neumayr, Nick Stracke, Melvin Sevi, Vincent Tao Hu, and Björn Ommer. Continuous, Subject-Specific Attribute Control in T2I Models by Identifying Semantic Directions. In *Proceedings of the IEEE/CVF Conference on Computer Vision and Pattern Recognition*, 2025. 1, 2, 3, 5
- [4] Jiankang Deng, Jia Guo, Xue Niannan, and Stefanos Zafeiriou. Arcface: Additive angular margin loss for deep face recognition. In *CVPR*, 2019. 4
- [5] Jiankang Deng, Jia Guo, Yuxiang Zhou, Jinke Yu, Irene Kotsia, and Stefanos Zafeiriou. Retinaface: Single-stage dense face localisation in the wild. *arXiv preprint arXiv:1905.00641*, 2019. 4, 5, 6, 12
- [6] Prafulla Dhariwal and Alexander Nichol. Diffusion models beat gans on image synthesis. *Advances in neural information processing systems*, 34:8780–8794, 2021. 2
- [7] Rinon Gal, Yuval Alaluf, Yuval Atzmon, Or Patashnik, Amit H Bermano, Gal Chechik, and Daniel Cohen-Or. An image is worth one word: Personalizing text-to-image generation using textual inversion. *arXiv preprint arXiv:2208.01618*, 2022. 12
- [8] Rinon Gal, Yuval Alaluf, Yuval Atzmon, Or Patashnik, Amit H. Bermano, Gal Chechik, and Daniel Cohen-Or. An image is worth one word: Personalizing text-to-image generation using textual inversion, 2022. 1, 2
- [9] Rohit Gandikota, Joanna Materzyńska, Tingrui Zhou, Antonio Torralba, and David Bau. Concept sliders: Lora adaptors for precise control in diffusion models. In *European Conference on Computer Vision*, pages 172–188. Springer, 2024. 1, 2, 3, 5
- [10] Ian Goodfellow, Jean Pouget-Abadie, Mehdi Mirza, Bing Xu, David Warde-Farley, Sherjil Ozair, Aaron Courville, and Yoshua Bengio. Generative adversarial networks. *Communications of the ACM*, 63(11):139–144, 2020. 2
- [11] Yuchao Gu, Xintao Wang, Jay Zhangjie Wu, Yujun Shi, Yunpeng Chen, Zihan Fan, Wuyou Xiao, Rui Zhao, Shuning Chang, Weijia Wu, et al. Mix-of-show: Decentralized low-rank adaptation for multi-concept customization of diffusion models. *Advances in Neural Information Processing Systems*, 36, 2024. 1, 2
- [12] Jia Guo and Jiankang Deng. Insightface: 2d and 3d face analysis project. <https://github.com/deepinsight/insightface>, 2018–2025. Accessed: 2025-03-04. 4
- [13] Erik Härkönen, Aaron Hertzmann, Jaakko Lehtinen, and Sylvain Paris. Ganspace: Discovering interpretable gan controls. *Advances in neural information processing systems*, 33:9841–9850, 2020. 2, 3
- [14] Jonathan Ho and Tim Salimans. Classifier-free diffusion guidance. *arXiv preprint arXiv:2207.12598*, 2022. 3
- [15] Jonathan Ho, Ajay Jain, and Pieter Abbeel. Denoising diffusion probabilistic models. *Advances in neural information processing systems*, 33:6840–6851, 2020. 2
- [16] Edward J Hu, Yelong Shen, Phillip Wallis, Zeyuan Allen-Zhu, Yuanzhi Li, Shean Wang, Lu Wang, and Weizhu Chen. LoRA: Low-rank adaptation of large language models. In *International Conference on Learning Representations*, 2022. 1, 2, 5, 12
- [17] Ben Hutchinson, Jason Baldridge, and Vinodkumar Prabhakaran. Underspecification in scene description-to-depiction tasks. *arXiv preprint arXiv:2210.05815*, 2022. 1
- [18] Tero Karras, Samuli Laine, and Timo Aila. A style-based generator architecture for generative adversarial networks. In *Proceedings of the IEEE/CVF conference on computer vision and pattern recognition*, pages 4401–4410, 2019. 2, 5, 12
- [19] Davis E King. Dlib-ml: A machine learning toolkit. *Journal of Machine Learning Research*, 10(Jul):1755–1758, 2009. 5, 6, 12
- [20] Diederik P Kingma. Auto-encoding variational bayes. *arXiv preprint arXiv:1312.6114*, 2013. 2, 4
- [21] Nupur Kumari, Bingliang Zhang, Richard Zhang, Eli Shechtman, and Jun-Yan Zhu. Multi-concept customization of text-to-image diffusion. In *Proceedings of the IEEE/CVF Conference on Computer Vision and Pattern Recognition*, pages 1931–1941, 2023. 2
- [22] Xiaoming Li, Xinyu Hou, and Chen Change Loy. When stylegan meets stable diffusion: a w+ adapter for personalized image generation. In *Proceedings of the IEEE/CVF Conference on Computer Vision and Pattern Recognition*, pages 2187–2196, 2024. 1, 2, 5
- [23] Nan Liu, Shuang Li, Yilun Du, Antonio Torralba, and Joshua B Tenenbaum. Compositional visual generation with composable diffusion models. In *European Conference on Computer Vision*, pages 423–439. Springer, 2022. 5, 7
- [24] Yun Luo, Zhen Yang, Fandong Meng, Yafu Li, Jie Zhou, and Yue Zhang. An empirical study of catastrophic forgetting in large language models during continual fine-tuning. *arXiv preprint arXiv:2308.08747*, 2023. 2
- [25] Michael McCloskey and Neal J Cohen. Catastrophic interference in connectionist networks: The sequential learning problem. In *Psychology of learning and motivation*, pages 109–165. Elsevier, 1989. 2
- [26] Alex Nichol, Prafulla Dhariwal, Aditya Ramesh, Pranav Shyam, Pamela Mishkin, Bob McGrew, Ilya Sutskever, and Mark Chen. Glide: Towards photorealistic image generation and editing with text-guided diffusion models. *arXiv preprint arXiv:2112.10741*, 2021. 1
- [27] Rishabh Parihar, VS Sachidanand, Sabariswaran Mani, Tejan Karmali, and R Venkatesh Babu. Precisecontrol: Enhancing text-to-image diffusion models with fine-grained attribute control. In *European Conference on Computer Vision*, pages 469–487. Springer, 2024. 1, 2
- [28] Alec Radford, Jong Wook Kim, Chris Hallacy, Aditya Ramesh, Gabriel Goh, Sandhini Agarwal, Girish Sastry,

- Amanda Askell, Pamela Mishkin, Jack Clark, et al. Learning transferable visual models from natural language supervision. In *International conference on machine learning*, pages 8748–8763. PMLR, 2021. 4, 6
- [29] Aditya Ramesh, Mikhail Pavlov, Gabriel Goh, Scott Gray, Chelsea Voss, Alec Radford, Mark Chen, and Ilya Sutskever. Zero-shot text-to-image generation. In *International conference on machine learning*, pages 8821–8831. Pmlr, 2021. 1
- [30] Robin Rombach, Andreas Blattmann, Dominik Lorenz, Patrick Esser, and Björn Ommer. High-resolution image synthesis with latent diffusion models, 2021. 1, 3
- [31] Nataniel Ruiz, Yuanzhen Li, Varun Jampani, Yael Pritch, Michael Rubinstein, and Kfir Aberman. Dreambooth: Fine tuning text-to-image diffusion models for subject-driven generation. 2022. 1, 2
- [32] Nataniel Ruiz, Yuanzhen Li, Varun Jampani, Yael Pritch, Michael Rubinstein, and Kfir Aberman. Dreambooth: Fine tuning text-to-image diffusion models for subject-driven generation. In *Proceedings of the IEEE/CVF conference on computer vision and pattern recognition*, pages 22500–22510, 2023. 12
- [33] Chitwan Saharia, William Chan, Saurabh Saxena, Lala Li, Jay Whang, Emily L Denton, Kamyar Ghasemipour, Raphael Gontijo Lopes, Burcu Karagol Ayan, Tim Salimans, et al. Photorealistic text-to-image diffusion models with deep language understanding. *Advances in neural information processing systems*, 35:36479–36494, 2022. 1
- [34] Sefik Ilkin Serengil and Alper Ozpinar. Hyperextended lightface: A facial attribute analysis framework. In *2021 International Conference on Engineering and Emerging Technologies (ICEET)*, pages 1–4. IEEE, 2021. 5, 6, 12
- [35] Yujun Shen, Ceyuan Yang, Xiaou Tang, and Bolei Zhou. Interfacegan: Interpreting the disentangled face representation learned by gans. *IEEE transactions on pattern analysis and machine intelligence*, 44(4):2004–2018, 2020. 2, 3, 5
- [36] Jascha Sohl-Dickstein, Eric Weiss, Niru Maheswaranathan, and Surya Ganguli. Deep unsupervised learning using nonequilibrium thermodynamics. In *International conference on machine learning*, pages 2256–2265. PMLR, 2015. 2
- [37] Kihyuk Sohn, Honglak Lee, and Xinchen Yan. Learning structured output representation using deep conditional generative models. *Advances in neural information processing systems*, 28, 2015. 2, 3, 4
- [38] Yang Song, Jascha Sohl-Dickstein, Diederik P Kingma, Abhishek Kumar, Stefano Ermon, and Ben Poole. Score-based generative modeling through stochastic differential equations. *arXiv preprint arXiv:2011.13456*, 2020. 3
- [39] Omer Tov, Yuval Alaluf, Yotam Nitzan, Or Patashnik, and Daniel Cohen-Or. Designing an encoder for stylegan image manipulation. *ACM Transactions on Graphics (TOG)*, 40(4): 1–14, 2021. 5
- [40] Zongze Wu, Dani Lischinski, and Eli Shechtman. Stylespace analysis: Disentangled controls for stylegan image generation. In *Proceedings of the IEEE/CVF conference on computer vision and pattern recognition*, pages 12863–12872, 2021. 2, 3
- [41] Enze Xie, Wenhai Wang, Zhiding Yu, Anima Anandkumar, Jose M Alvarez, and Ping Luo. Segformer: Simple and efficient design for semantic segmentation with transformers. In *Neural Information Processing Systems (NeurIPS)*, 2021. 6
- [42] Yang Yang, Wen Wang, Liang Peng, Chaotian Song, Yao Chen, Hengjia Li, Xiaolong Yang, Qinglin Lu, Deng Cai, Boxi Wu, et al. Lora-composer: Leveraging low-rank adaptation for multi-concept customization in training-free diffusion models. *arXiv preprint arXiv:2403.11627*, 2024. 1, 2
- [43] Hu Ye, Jun Zhang, Sibio Liu, Xiao Han, and Wei Yang. Ip-adapter: Text compatible image prompt adapter for text-to-image diffusion models. 2023. 2, 3, 9
- [44] Cheng Zhang, Xuanbai Chen, Siqi Chai, Chen Henry Wu, Dmitry Lagun, Thabo Beeler, and Fernando De la Torre. Itigen: Inclusive text-to-image generation. In *Proceedings of the IEEE/CVF International Conference on Computer Vision*, pages 3969–3980, 2023. 1, 2, 5, 7
- [45] Brian Nlong Zhao, Yuhang Xiao, Jiashu Xu, Xinyang Jiang, Yifan Yang, Dongsheng Li, Laurent Itti, Vibhav Vineet, and Yunhao Ge. Dreamdistribution: Prompt distribution learning for text-to-image diffusion models. 2023. 2
- [46] Tiancheng Zhao, Ran Zhao, and Maxine Eskenazi. Learning discourse-level diversity for neural dialog models using conditional variational autoencoders. In *Proceedings of the 55th Annual Meeting of the Association for Computational Linguistics (Volume 1: Long Papers)*. Association for Computational Linguistics, 2017. 2, 3, 4

## A. Evaluation Details

**Dataset and Preprocessing** **FFHQ**: FFHQ [18] is a high-quality public face dataset. To use the data for finetuning Text-to-image diffusion models, we get a caption per image by using ChatGPT [1]. We preprocessed 20 facial attributes: 13 attributes for facial compositions, one attribute for age, and 6 attributes for race.

Specifically, we first obtain head pose information (pitch, roll, and yaw)<sup>4</sup> and use them to get frontal view face images; We extract 16,336 images out of 70,000 images, which are used as our fine-tuning data. Next, we use 68 landmarks per image from dlib [19] to obtain the information about facial composition. For example, to obtain ‘the gap between eyes’, we use the 39th and 42nd landmarks coordinates and compute the L1 norm. Min-max normalization is applied to make the range of the value within 0 to 1, which means that 1 and 0 respectively indicate the max and min values of a certain attribute from the fine-tuning dataset. The 13 attributes related to facial compositions are: ‘the gap between eyes’, ‘width of eyes’, ‘height of eyes’, ‘width of nose’, ‘height of nose’, ‘width of mouth’, ‘height of mouth’, ‘width of face’, ‘height of face’ (from glabella to chin), ‘height between eyebrow and eye’, ‘height between nose and mouth’, ‘height between mouth and chin’, and ‘width of eyebrow’.

For age and race extraction, we use deepface [34] with a detector Retinaface [5]. The age is divided by 100 for normalization purposes. The six extracted features about the race are ‘p(Asian)’, ‘p(Black)’, ‘p(Hispanic Latino)’, ‘p(Indian)’, ‘p(Middle Eastern)’, ‘p(White)’.

**EVOX**: We used a commercial grade vehicle image dataset from EVOX<sup>5</sup> as the experiment data. The dataset includes high-resolution images across multiple car models collected from 2018 to 2023, totally 2030 images.

**Predefined 30 text prompts for evaluation** ‘A smiling man’, ‘A smiling woman’, ‘A man surprised’, ‘A woman surprised’, ‘An angry man’, ‘An angry woman’, ‘A man crying’, ‘A woman crying’, ‘A sad man’, ‘A sad woman’, ‘A painting of a man’, ‘A painting of a woman’, ‘A marble sculpture of a man’, ‘A marble sculpture of a woman’, ‘A 3D model of a man’, ‘A 3D model of a woman’, ‘A man wearing earrings’, ‘A woman wearing earrings’, ‘A man with a crown’, ‘A woman with a crown’, ‘A man wearing a cap’, ‘A woman wearing a cap’, ‘A man wearing eyeglasses’, ‘A woman wearing eyeglasses’, ‘A man with rainbow hair’, ‘A woman with rainbow hair’, ‘A man with shadow fade hair style’, ‘A woman with ponytail’, ‘A man

wearing a furry cat ears headband’, ‘A woman wearing a furry cat ears headband’.

**Test data creation for the evaluation for the baselines (Latent Control)**. The 13 attributes that we preprocessed from FFHQ are used to measure single attribute performance. The multi-attributes that we used to measure are as followings: (‘height\_between\_eyebrow\_eye’, ‘width\_of\_face’), (‘width\_of\_mouth’, ‘height\_of\_face’), (‘width\_of\_nose’, ‘height\_of\_mouth’), (‘height\_between\_mouth\_chin’, ‘gap\_between\_eyes’), (‘height\_of\_face’, ‘height\_of\_eyes’), (‘width\_of\_eyes’, ‘width\_of\_face’), (‘width\_of\_nose’, ‘height\_of\_eyes’), (‘width\_of\_nose’, ‘gap\_between\_eyes’), (‘width\_of\_eyebrow’, ‘height\_between\_nose\_mouth’), (‘height\_of\_nose’, ‘width\_of\_eyes’). We generate a positive and a negative pair from each attribute set and compare the CR and DIS scores as mentioned in the main paper.

**Test data creation for the evaluation for the baselines (Absolute Control)**. For each prompt, we randomly sample 50 combinations of 20 attributes. As a result, the attribute combinations for testing contains 1,500 samples; 30 (text prompts) by 50 (20-dimensional attributes combinations per prompt). Specifically, for facial composition attributes, we first obtain the means and the standard deviations of the attributes from the finetuning data. For example, the mean of ‘gap between eyes’ is 0.687 and the standard deviation is 0.087. We sample from 2 sigma region. For age, we sample from normal distribution of which mean and standard deviation is 30 and 10. For race, we uniformly sample from 0.8 and 1 to assign the biggest value to one of 6 races. Once the major race is determined, the values for other races are randomly assigned to be sum-to-one.

## B. Application results: LoRA

LoRA can be used for personalizing pretrained Diffusion Models [7, 16, 32]. In this section, we show that Att-Adapter can be combined with the LoRA module that is finetuned for the appearance of a specific individual. Briefly, we used 22 images of a certain celebrity (Jennifer Lawrence) to finetune LoRA. After finetuning, we combine LoRA and Att-Adapter which are separately trained. The results are shown in Fig. 12. We can see that Att-Adapter can adjust the facial components of the generated image while the person identity is heavily affected by LoRA module. This shows that the wide applicability of Att-Adapter.

<sup>4</sup><https://github.com/DCGM/ffhq-features-dataset>

<sup>5</sup>The images used in this study are the property of EVOX Productions, LLC and are subject to copyright law. The appropriate licenses and permissions have been obtained to ensure the rightful use of these images in our study. For more information, see <https://www.evostock.com/>.

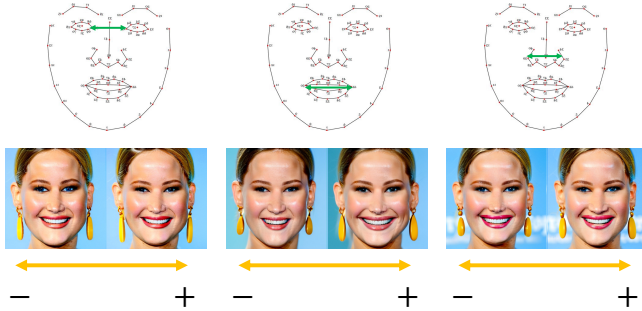


Figure 12. Qualitative experiments showing that LoRA and Att-Adapter can be combined during the sampling process.

### C. Exploring training settings.

In this section, we explore some of the important factors that could be needed during the training process for Att-Adapter.

**Training iteration** First we analyze the quantitative performance per iteration which is shown in Table 7. We can see the trade-off between the finetuned knowledge and pretrained knowledge as iteration goes on. At 100k, we can better maintain the pretrained knowledge. However, the performance w.r.t. finetuned knowledge is not good. After 200k, even though we lose some pretrained knowledge, we get better scores for the finetuned knowledge. It is not easy to determine which checkpoint is better among 200k and 300k as their performance gap is not conspicuous. During the experiments, we empirically used the model saved at 200k.

(Iter.)	Finetuned knowledge ( $\downarrow$ )			Pretrained knowledge ( $\uparrow$ )	
	Facial comp.	Age	Race	CLIP	ChatGPT
100k	21.1	9.8	2.48	<b>0.285</b>	<b>82%</b>
200k	<b>15.57</b>	8.0	<b>0.36</b>	0.283	78%
300k	15.92	<b>7.7</b>	<b>0.36</b>	0.282	77%

Table 7. Performance per iterations. We observe that the performance is empirically converged around 200k.

**Embedding dimension of  $Z$ .** Second, we explore the impact of dimensionality of  $Z$  on performance in Table 8. Interestingly, with 128 dimension, Att-Adapter tend to learn less the finetuned knowledge while maintaining more the pretrained knowledge. With 512 dimension, the model shows decent performance in both finetuned and pretrained knowledge. With 2048 dimension, the model shows comparable performance with the 512 setting; The age prediction gets slightly better, but slightly worse in most of the other measures.

**Non-isotropic gaussian prior.** Lastly, we compare the performance of using isotropic/non-isotropic gaussian for

(Dim.)	Finetuned knowledge ( $\downarrow$ )			Pretrained knowledge ( $\uparrow$ )	
	Facial comp.	Age	Race	CLIP	ChatGPT
128	20.54	9.3	0.808	<b>0.285</b>	<b>83%</b>
512	<b>17.42</b>	8.5	<b>0.799</b>	0.282	80%
2048	17.53	<b>7.7</b>	0.987	0.282	75%

Table 8. Performance comparisons given different  $Z$  dimensions. For each setting, the checkpoint saved at 150k iterations is used.

prior distribution. For isotropic gaussian, we estimate a scalar. For non-isotropic setting, we estimate a vector (i.e., the diagonal term of the covariance matrix.) The results are shown in Table 9. At 100k, we can see that the non-isotropic setting is better than the isotropic setting for learning the finetuned knowledge. We conjecture that this is because the higher degree of freedom of non-isotropic gaussian (than the isotropic gaussian) could be beneficial at fitting at some points. At 200k and 300k, however, the difference gets smaller and both settings become comparable. We empirically used the isotropic gaussian prior setting for our main experiments.

(Iter.)	Finetuned knowledge ( $\downarrow$ )			Pretrained knowledge ( $\uparrow$ )	
	Facial comp.	Age	Race	CLIP	ChatGPT
100k	<b>-0.39</b>	<b>-0.4</b>	<b>-0.663</b>	0.0	0%
200k	+0.39	<b>-0.2</b>	+0.207	-0.001	-1%
300k	<b>-0.23</b>	<b>-0.1</b>	+0.076	0.0	<b>+2%</b>

Table 9. Performance comparisons of two settings; 1. isotropic gaussian for the prior, 2. non-isotropic gaussian for the prior distribution. The values in the table are obtained by subtracting the values of the second setting from the values of the first setting, i.e., (informally) iso value – noniso value.

### D. Additional comparison of Att-Adapter and LoRA

Fig. 13 shows the advantage of our method straightforward. Each column shows the result from the different conditioning value for the given attribute. For each macro column, we can observe from the center two rows that both Att-Adapter and LoRA show good performance given the within-domain conditioning values, i.e.,  $[0, 1]$ . However, only Att-Adapter can deal with the negative or greater-than-one conditioning. This is because LoRA is only trained with dealing with the discretized and tokenized string identifiers of 0,1,...,9. For example, given -0.55 from the leftmost column, our pre-processor for discretizing makes the value -5. We guess LoRA ignores ‘-’ sign, and ‘5’ is taken, which yields the eyes openness to the similar extent with the third column (i.e., 0.59). Similarly, given 1.10 in the fourth column from the left, our discretizer makes it 11, which becomes ‘1’ and ‘1’ after tokenized. We can see that LoRA recognizes the two ‘1’s as ‘1’ by comparing the eye openness with the second column (i.e., 0.14, 1 after discretized). On the other

hand, as shown in the first row, Att-Adapter can extrapolate to the attribute values beyond  $[0, 1]$ , to the unseen domain.

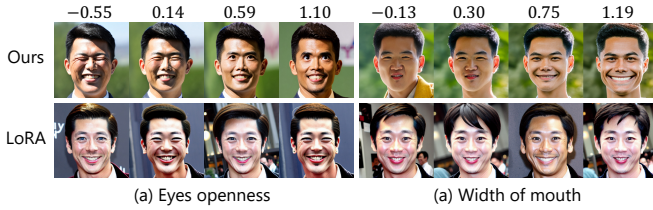


Figure 13. Extrapolation comparisons with LoRA showing the strength of Att-Adapter. A prompt of “A stylish man smiling” is used with ‘Asian’ condition.

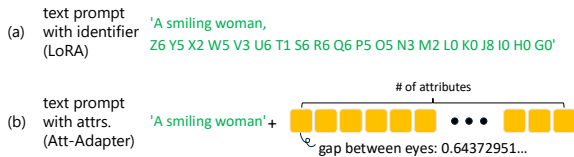


Figure 14. Visualization of the input setting of LoRA baseline. All the continuous attributes are discretized and named as special tokens. For example, the attribute ‘gap between eyes’ and its value 0.64 becomes ‘Z6’. Multi-attributes are linearly converted and added consecutively.

## E. Additional Analysis

### E.1. Challenging attributes

In this section, we show that Att-Adapter can be used beyond frontal-view images. In order to show this, we extend our training dataset from the frontal-view face images to the entire FFHQ dataset. We also additionally add three attributes; yaw, pitch, and roll<sup>6</sup>. The results are shown in Fig. 15. Interestingly, even though Att-Adapter is not specifically designed for understanding 3D domain, we can see that the left-right rotation (i.e., yaw) and the up-down rotation (i.e., pitch) can be controlled. However, we observed that roll is not controllable. To improve this, we believe additional facial dataset with diverse roll information is required as FFHQ face-cropped dataset is face aligned. We also think it would be interesting and powerful if 3D domain knowledge could be aggregated in Att-Adapter which is beyond our research scope.

Additionally, we show that Att-Adapter can control two attributes simultaneously in Fig. 16.



Figure 15. Qualitative results on additional attributes control. The results are generated by taking a prompt of “A smiling woman”.

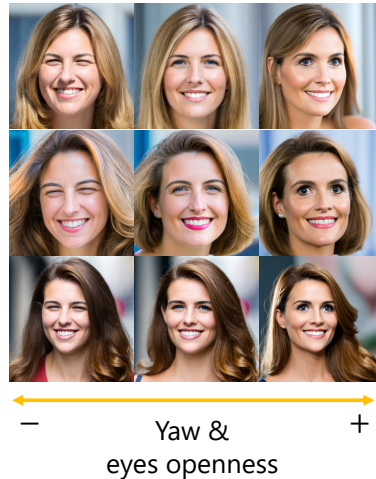


Figure 16. Additional two-attributes controlling examples. A prompt of “A smiling woman” is used.

<sup>6</sup><https://github.com/DCGM/ffhq-features-dataset>